Optimized production of hyperpolarized ^{129}Xe at 2 bars for in vivo lung magnetic resonance imaging

Graham Norquay, Steven R. Parnell, Xiaojun Xu, Juan Parra-Robles, and Jim M. Wild

Citation: Journal of Applied Physics **113**, 044908 (2013); doi: 10.1063/1.4776763
View online: https://doi.org/10.1063/1.4776763
View Table of Contents: http://aip.scitation.org/toc/jap/113/4
Published by the American Institute of Physics

Optimized production of hyperpolarized ^{129}Xe at 2 bars for *in vivo* lung magnetic resonance imaging

Graham Norquay, Steven R. Parnell,[a] Xiaojun Xu, Juan Parra-Robles, and Jim M. Wild[b]
Unit of Academic Radiology, University of Sheffield, Sheffield, South Yorkshire, S10 2JF United Kingdom

(Received 30 March 2012; accepted 2 January 2013; published online 31 January 2013)

In this work, the production rate of a spin-exchange optical pumping ^{129}Xe gas polarizer was optimized for routine generation of hyperpolarized ^{129}Xe for *in vivo* lung MRI. This system uses a narrow ($\sim$0.1 nm linewidth), tuneable external cavity laser (operating at $\sim$25 W) for SEOP of 3% gas mixtures of Xe inside a mid-pressure (2 bars) cell of 491 cm^3 volume. Under this regime, theoretical and experimentally measured ^{129}Xe polarizations were calculated to be 24% and 12%, respectively, for a gas flow rate of 300 sccm and a cell temperature of 373 K. The photon efficiency was evaluated, yielding theoretical and experimental values of 0.039 and 0.046, respectively. The theoretical efficiency was calculated from spin-exchange and spin-destruction cross sections and the experimental photon efficiency was measured under flow for a gas-cell residency time equal to an empirically determined spin-exchange time of 45 s. In addition, details of the Xe freeze-out process were analyzed with a model of polarization decay during Xe accumulation in the frozen phase, where a T_1 of 87 ± 2 min was observed. To demonstrate the system's application, *in vivo* lung magnetic resonance images (signal-to-noise ratio $\sim$ 50 from a voxel of 15 mm$\times$ 4 mm$\times$ 4 mm) were acquired using modest volumes (<400 ml) of isotopically enriched (86% ^{129}Xe) Xe gas polarized to >10%. Despite the experimental polarization being a factor of 2 lower than the predicted polarization for typical operating parameters, the system is close to the theoretical photon efficiency and the system has so far produced polarized gas for more than 100 *in vivo* ^{129}Xe lung imaging studies. © *2013 American Institute of Physics*. [http://dx.doi.org/10.1063/1.4776763]

I. INTRODUCTION

The nuclear spin of the inert gas isotopes ^{3}He and ^{129}Xe can be hyperpolarized (HP) by spin-exchange with a vapour of a polarized alkali metal such as rubidium, whose valence electrons have been spin polarized by laser optical pumping (OP).[1] Once hyperpolarized, these gases can be inhaled to non-invasively study lung structure and function[2,3] with magnetic resonance imaging (MRI). HP ^{3}He gas MRI has been evaluated in multiple clinical studies in different lung diseases and has been shown to have sensitivity to early stage lung disease such as early smoking related emphysema[4,5] and early obstruction of the airways in pediatric cystic fibrosis.[6]

Global supplies of ^{3}He are limited,[7] whereas Xe can be extracted from air, hence ^{129}Xe lung MRI[8] offers a potentially cheaper and more sustainable alternative to ^{3}He for clinical lung imaging. Naturally abundant Xe in the air consists of several different isotopes and enrichment can be used to provide a higher concentration of ^{129}Xe. As well as being chemically inert, Xe has the property of being soluble in many fluids and biological tissues and its resonance has a highly environment-sensitive chemical shift. Thus, dissolved-phase ^{129}Xe NMR can provide valuable insight into the various gas- and dissolved-phase exchange mechanisms occurring within the lung and other perfused organs.[9–11] Preliminary clinical studies with ^{129}Xe lung MRI[12,13] suggest that the gas could have comparable functional sensitivity to lung diseases as ^{3}He MRI.

Crucial to the success of gas and dissolved-phase imaging with HP ^{129}Xe is the production of volumes of gas (0.3-1 l) with high levels of polarization. As such, reduction of inhaled Xe volume and maximization of polarization is paramount. For clinical translation, robust, on-demand production of HP ^{129}Xe at high polarization is also desirable.

Optimization of the spin-exchange optical pumping (SEOP) parameters, temperature and gas flow rate through the cell, has been done for both low-[14,15] and high-pressure systems.[16,17] In this work, these two parameters were optimized for a SEOP system operating at mid-range total cell pressure of 2 bars with 3% Xe concentrations with a narrow ($\sim$0.1 nm) linewidth laser. Theoretical ^{129}Xe polarizations for this system are compared with experimentally measured values and the photon efficiency of SEOP in this regime is also evaluated. To demonstrate the end application, *in vivo* lung images were obtained using varying volumes and polarizations of ^{129}Xe that had been polarized with different flow rates and accumulation times.

A. Spin-exchange optical pumping background

The technique used to polarize the nuclei of ^{129}Xe gas atoms is SEOP,[1] whereby Rb valence electrons are optically pumped with circularly polarized laser light resonant on the D_1 transition line (794.77 nm in air), resulting in a highly polarized electron spin Zeeman ground state. Within a SEOP cell, collisions between ^{129}Xe and Rb atoms transfer spin polarization from the Rb electrons to the ^{129}Xe nuclei via hyperfine interactions.[18] To increase the efficiency of the optical pumping process, N_2 and He are added to the cell to

[a]Present address: Center for Exploration of Energy and Matter, University of Indiana, USA.
[b]j.m.wild@sheffield.ac.uk.

act as buffer gases. N_2 prevents radiative emissions of uncontrolled circularly polarized or linearly polarized photons by quenching the Rb excited energy state into its vibrational levels,[19] while He, with its lower Rb spin-destruction rate, is used at higher concentrations than N_2 and, through collisional broadening, causes an increase in the linewidth of the D_1 absorption line.[20]

The Rb polarization, P_{Rb}, at a position z along the pumping axis in the cell is given by[21]

$$P_{Rb}(z) = \frac{\gamma_{opt}(z)}{\gamma_{opt}(z) + \Gamma_{SD}}, \quad (1)$$

where γ_{opt} is the optical pumping rate, which is dependent on the photon absorption cross section, σ_s, and on the photon flux from the laser, Φ, within the cell. γ_{opt} is given by

$$\gamma_{opt}(\nu, z) = \int \Phi(\nu, z)\sigma_s(\nu)d\nu. \quad (2)$$

Γ_{SD} represents the Rb spin polarization destruction rate, which can be attributed to binary collisions with atoms in the SEOP mixture or the formation and breakup of short-lived Rb-Xe van der Waals molecules (vdW). It is given by

$$\Gamma_{SD}^{BC} = \sum_i [G_i]\kappa_{SD}^{Rb-i}, \quad (3)$$

where κ_{SD}^{Rb-i} is the Rb spin-destruction cross section for Rb binary collisions with each gas atom present in the SEOP cell, each with an atomic density given by $[G_i]$. Values for κ_{SD}^{Rb-i} have been reported as $\kappa_{SD}^{Rb-Rb} = 4.2 \times 10^{-13}$ cm^3 s^{-1},[22] $\kappa_{SD}^{Rb-He} = 1 \times 10^{-29}\, T^{4.26}$ cm^3 s^{-1},[22] $\kappa_{SD}^{Rb-N_2} = 1.3 \times 10^{-25}\, T^3$ cm^3 s^{-1},[23] and $\kappa_{SD}^{Rb-Xe} = 6.3 \times 10^{-17}(T - 273.15)^{1.17}$ cm^3 s^{-1},[24] where T is the temperature in K. See Table I for comparative magnitudes of each cross section for a cell temperature of 373 K. The Rb-Xe spin-destruction cross section was obtained from a measured cross section of 8.48×10^{-15} cm^3 s^{-1} at 253 K,[24] where a $(T - 273)^{1.17}$ temperature dependence was observed. The Rb spin-destruction rate due to the formation and breakup of Rb-Xe vdW collisions has been estimated[25] as

$$\Gamma_{SD}^{vdW} = \left(\frac{66183}{1 + 0.92\frac{[N_2]}{[Xe]} + 0.31\frac{[He]}{[Xe]}}\right)\left(\frac{T}{423}\right)^{-2.5}. \quad (4)$$

The total Rb spin-destruction rate is then $\Gamma_{SD} = \Gamma_{SD}^{BC} + \Gamma_{SD}^{vdW}$, and a value for a gas-composition-specific vdW spin-destruction cross section, κ_{SD}^{vdW}, can be calculated as 1.79×10^{-16} cm^3 s^{-1} from $\Gamma_{SD}^{vdW}/[G_{tot}]$ where $[G_{tot}] = \sum_i [G_i] = [Xe] + [N_2] + [He]$ is the total gas density within the SEOP cell used in this study (see Table I). From Eqs. (3) and (4), it is clear that in order to reduce the Rb spin-destruction, the Xe concentration should be kept low within the cell, whereas He and N_2 can be held at higher pressures, due to their spin-destruction cross sections being orders of magnitude smaller than that of Xe (Table I).

The nuclear spin polarization of ^{129}Xe generated through spin-exchange with polarized Rb electrons during gas flow after a residency time, t_{res}, in the cell is given by[16]

$$P_{Xe}^{cell}(t_{res}) = \frac{\gamma_{SE}}{\gamma_{SE} + \Gamma}\langle P_{Rb}\rangle(1 - e^{-(\gamma_{SE}+\Gamma)t_{res}}), \quad (5)$$

where Γ is the rate of loss of nuclear ^{129}Xe polarization, γ_{SE} denotes the Rb-Xe spin-exchange rate, and $\langle P_{Rb}\rangle$ is the average Rb polarization in the cell. Γ is thought to be dominated by wall relaxation, which depends on the cell geometry (surface area/volume) and its surface relaxation properties (paramagnetic centers).[26] γ_{SE} is dominated by Rb-Xe binary collisions at high pressure[27,28] and short-lived Rb-Xe vdW interactions at low pressure.[29] Combining the formula for the Rb-Xe spin-exchange rate due to the contribution from Rb-Xe vdW molecules, γ_{SE}^{vdW} and the contribution from Rb-Xe spinexchange due to binary collisions, γ_{SE}^{BC}, the total theoretical spin-exchange rate, γ_{SE}^{theory}, can be calculated from[29]

$$\gamma_{SE}^{theory} = \gamma_{SE}^{vdW} + \gamma_{SE}^{BC} = \left(\sum_i \frac{1}{\left(\frac{[G_i]}{\xi_i}\right)} + \kappa_{SE}^{Rb-Xe}\right)[Rb]$$
$$= (\kappa_{SE}^{vdW} + \kappa_{SE}^{BC})[Rb]. \quad (6)$$

The parameter ξ_i denotes vdW-specific rates for each gas atom with density $[G_i]$. $\xi_{Xe} = 5230$ Hz;[29] $\xi_{N_2} = 5700$ Hz, calculated by Rice and Rafferty[30] from Zeng *et al.*;[31] and $\xi_{He} = 17\,000$ Hz, calculated by Driehuys *et al.*[16] from Cates *et al.*[29] κ_{SE}^{vdW} and κ_{SE}^{BC} are the spin-exchange cross sections from vdW interactions and binary Rb-Xe collisions, respectively. κ_{SE}^{vdW} was calculated from the summation term in Eq. (6) as 3.46×10^{-16} cm^3 s^{-1} (specific to the gas composition used in this study) and κ_{SE}^{BC} has been

TABLE I. Upper half: calculated number densities of atoms in the cell and binary spin-destruction cross sections, κ_{SD}^{Rb-i}. Lower half: vdW and binary spin-destruction and spin-exchange rates. All cross sections and rates correspond to a SEOP cell at a temperature 373 K, pressure of 2 bars (temperature and pressure of the cell when filling it with the gas mixture, total gas number density of 1.44 amg) and a gas composition of 3% Xe, 10% N_2, and 87% He.

Cell constituent	Rb	He	N_2	Xe
Atomic density (cm^{-3})	5.82×10^{12} (Ref. 32)	3.38×10^{19}	3.88×10^{18}	1.16×10^{18}
κ_{SD}^{Rb-i} (cm^3 s^{-1})	4.2×10^{-13} (Ref. 22)	9.04×10^{-19} (Ref. 22)	6.75×10^{-18} (Ref. 23)	1.37×10^{-14} (Ref. 24)
Interaction	Symbol	Spin-destruction rate (Hz)	Symbol	Spin-exchange rate (Hz)
Binary	Γ_{SD}^{BC}	1.27×10^4 Eq. (3)	γ_{SE}^{BC}	1.26×10^{-3} Eq. (6)
vdW	Γ_{SD}^{vdW}	6.94×10^3 Eq. (4)	γ_{SE}^{vdW}	2.01×10^{-3} Eq. (6)
Total	Γ_{SD}	1.97×10^4	γ_{SE}^{theory}	3.28×10^{-3}

reported as 2.17×10^{-16} cm^3 s^{-1}.[27] It is interesting to note in this regime that the vdW spin-exchange cross section is a factor of 1.6 larger than the binary spin-exchange cross section.

The binary spin-exchange term of Eq. (6), $\kappa_{SE}^{BC}[Rb]$, is independent of gas density, whereas the vdW term is inversely proportional to gas density. Since all terms are linear with [Rb], this suggests it is beneficial to operate at a low total gas density and a high Rb density, which can be achieved by decreasing the cell pressure and increasing the temperature. However, according to Eq. (3), increasing the cell temperature increases the binary Rb spin-destruction rate, while lowering the Xe density decreases the binary spin-destruction rate. Equation (4) indicates a decrease in the vdW Rb spin-destruction rate, Γ_{SD}^{vdW}, with decreasing temperature. It is worth noting that Γ_{SD}^{vdW} is independent of the total gas density and depends instead upon the composition of the gas mixture. Lowering the total gas pressure in the cell has the effect of decreasing the D_1 absorption linewidth, thereby decreasing the photon absorption efficiency for laser emission of fixed linewidth[20] and hence decreasing the optical pumping rate, γ_{opt} (Eq. (2)). This, as a result, decreases the average Rb polarization, $\langle P_{Rb} \rangle$, which in turn reduces the ^{129}Xe nuclear spin polarization (Eq. (5)). Equations (2)–(6) therefore indicate a complicated trade-off between Rb laser light absorption, Rb spin-destruction and Rb-Xe spin-exchange rates for temperature, pressure and gas density changes in the cell.

The method most commonly used to obtain high volumes of polarized ^{129}Xe is referred to as "continuous flow" mode. Made feasible for large volume ^{129}Xe polarization by Driehuys *et al.*,[16] continuous flow SEOP utilizes the fast spin-exchange rate between Rb and Xe. The method used by Driehuys *et al.* operates with a high gas density (>5 amg) cell combined with broad linewidth lasers (~2 nm FWHM available at the time) for optical pumping. The combination of broad linewidth lasers and a pressure-broadened Rb D_1 absorption line provides a good emission/absorption linewidth match, enabling efficient absorption of the polarized beam of photons from the laser. To mitigate Rb-Xe spin destruction at these high pressures (see Eq. (3)), low Xe partial pressure is needed in the cell, which means that for high-volume Xe production, the ^{129}Xe needs to be polarized at low partial pressures and cryogenically collected using a liquid nitrogen freeze-out process. During freeze-out, Xe is separated from the buffer gases, He and N_2, and accumulates over time as frozen ice in a constant gas flow regime. This requires gas to be frozen out over a period of 30-60 min, typically providing 1 l of polarized gas with polarizations of 5%-10%. The gas polarized with this system has been demonstrated to provide diagnostic quality ^{129}Xe lung MRI images in clinical lung imaging studies.[12]

An alternative approach developed at the University of New Hampshire[33] operates at low cell densities (<1 amg) using a very high power array (>1000 W) of narrow linewidth lasers. This system produces ^{129}Xe gas at high polarization and very promising clinical lung MRI results have been reported.[13] Nevertheless, the low-pressure regime still necessitates cryogenic collection of the Xe, or alternatively some method of compression would have to be used. Moreover, the complicated glassware, low-pressure regime and complex high power laser system means that this system is expensive to build and is maintenance intensive. At low pressures (0.01–1 amg), the formation and breakup times of vdW molecules are sufficiently long that the spin polarization can be completely lost during a molecular lifetime and is referred to as the long molecular lifetime limit.[24] This long molecular lifetime regime is characterized by a rapid increase in the spin-relaxation rate with increasing gas density due to increasing rates of molecular formation. At higher densities (1–10 amg), the relaxation becomes density independent as the increasing formation rate is compensated by a small relaxation probability in a single, short molecular lifetime. This is referred to as the short molecular lifetime limit and is the SEOP regime that is explored in this study where the total gas number density in the cell is 1.44 amg.

II. MATERIALS AND METHODS

A. Polarizer

The principal components of the polarizer are as follows:

(i) a Helmholtz B_0 coil (diameter 80 cm, $B_0 \sim 2.7$ mT).
(ii) A cylindrical Pyrex optical cell (25 cm length, 5 cm diameter) filled with <1 g of molten rubidium that was pipetted into the cell inside an argon gas glove box. The cell is located at the isocenter of the B_0 field within a non-magnetic ceramic hot-air oven with glass windows and has been in use with reliable results for ~1 yr. In order to examine cell wall relaxation effects, the T_1 of the ^{129}Xe in the cell was measured cold ($T \sim 293$ K) in order to limit effects of Rb spin-exchange from distorting the measurement. A gas T_1 of 48 ± 1 min using enriched (86% ^{129}Xe) Xe was observed in an optical pumping B_0 field of 2.7 mT using a home-built NMR system[34] with a surface RF coil placed on the top of the cell. From this, it can be concluded that cell wall relaxation is not significant.
(iii) An external cavity diode laser (ECDL) (based on the design of Chann *et al.*[35] and constructed in house) was used for optical pumping (see Fig. 1). The laser emission was centred on 794.77 nm and the FWHM was measured to be 0.09 ± 0.01 nm.[36]

For the generation of all HP ^{129}Xe samples, a gas mixture of 3% isotopically enriched Xe (86% ^{129}Xe), 10% N_2, and 87% He (Spectra Gases, UK) was flowed through the cell using a mass flow controller (Aalborg, Caché, Denmark), with a total gas pressure of 2 bars. The temperature of the cell was maintained at around 373 ± 1 K by flow of hot air through the ceramic-walled oven.

B. Polarization measurement

The cell temperature was first optimized under flow-mode. 3% Xe samples were collected directly from the cell at two different flow rates (300 and 500 sccm) by dispensing the SEOP gas mixture into a 1 l Tedlar plastic bag (Jensen, Coral Springs, Fl). The bag was then transported to

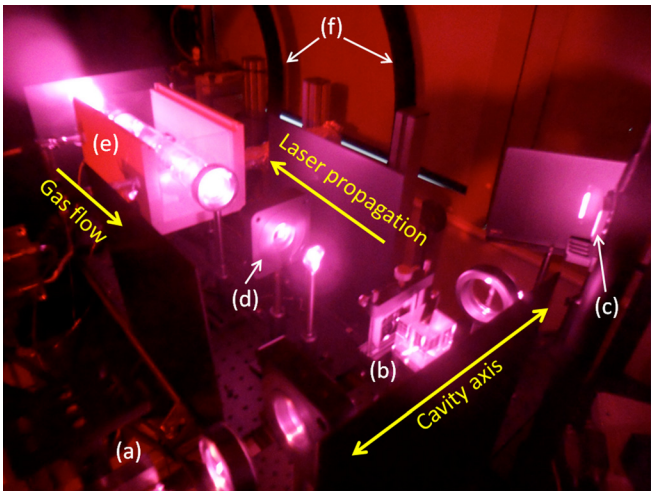

FIG. 1. SEOP apparatus. (a) laser diode bar; (b) beam-splitter cube (1/3 feedback along cavity axis, 2/3 transmission along cell axis); (c) holographic grating; (d) $\lambda/4$-wave plate; (e) ceramic oven for housing cell (lid removed); (f) B_0 coils.

a 1.5 T GE HDx system (GE Healthcare, Milwaukee, WI), whereupon 10 ml samples were decanted into an evacuated plastic syringe. Transport to the MR system took approximately 2 min and polarization losses were measured to be negligible (<1%). A free induction decay (FID) signal from the syringe sample was recorded following a 10° RF excitation pulse using a homebuilt saddle coil of 7.5 cm length and 3 cm diameter, tuned to resonate at a frequency of 17.66 MHz. Each FID was deliberately acquired with a low flip angle (FA) to ensure radiation damping effects were avoided.[37,38] This process was repeated with different cell temperatures and the optimum temperature for the two gas flow rates of 300 and 500 sccm was found to be 373 K (Fig. 2).

The signal from the HP ^{129}Xe samples was calibrated using the signal from a thermal ^{129}Xe sample (syringe containing 5 ml enriched Xe (86% ^{129}Xe), 5 ml oxygen, $T_1 \sim 6$ s)—see Figs. 3(a) and 3(b). The thermally polarized signal was obtained by averaging 100 pulse-acquisitions (TR = 35 s, FA = 90°). The polarization, $P_{\mathrm{Xe}}^{\mathrm{cell}}$, of the HP ^{129}Xe sample collected from the cell at a given flow rate was then calculated using

$$P_{\mathrm{Xe}}^{\mathrm{cell}} = \frac{S_{\mathrm{HP}}}{S_{\mathrm{therm}}} \frac{\sin(\alpha_{\mathrm{therm}})}{\sin(\alpha_{\mathrm{HP}})} \frac{\varepsilon_{\mathrm{therm}}}{\varepsilon_{\mathrm{HP}}} \frac{V_{\mathrm{therm}}}{V_{\mathrm{HP}}} P_{\mathrm{Boltz}}, \qquad (7)$$

where S_{HP} and S_{therm} are the FID signal amplitudes from HP ^{129}Xe and thermally polarized ^{129}Xe gas samples, respectively; α_{HP} and α_{therm} represent the respective flip angles used in acquiring signals; $\varepsilon_{\mathrm{HP}}$ and $\varepsilon_{\mathrm{therm}}$ denote the isotopic abundances of ^{129}Xe within the ^{129}Xe samples; V_{HP} and V_{therm} are the volumes of Xe gas in the samples; and P_{Boltz} is the ^{129}Xe Boltzmann polarization ($P_{\mathrm{Boltz}} = 1.45 \times 10^{-6}$ for ^{129}Xe nuclei at a B_0 field of 1.5 T at a temperature of 293 K).

The advantage of using this method is that, because the sample is located in the bore of the MR system, the polarization calculated reflects what the *in situ* ^{129}Xe polarization

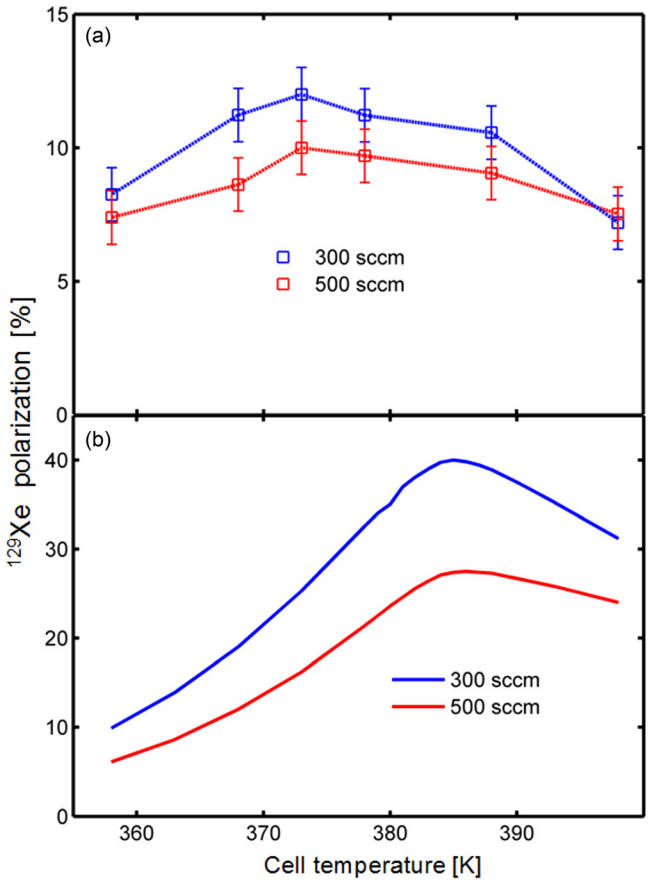

FIG. 2. (a) Experimental ^{129}Xe polarization vs. cell temperature at gas flow rates of 300 and 500 sccm. HP ^{129}Xe (samples obtained without cryogenic accumulation) signals were measured in the 1.5 T system. NB: blue and red lines are guides for the eye. (b) Modeled polarization vs. cell temperature.

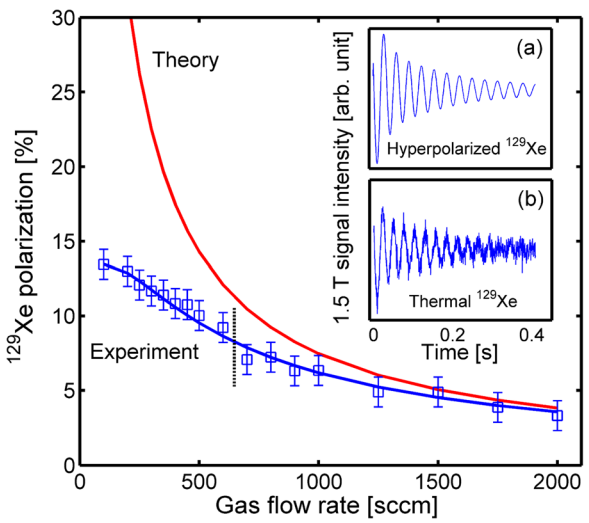

FIG. 3. ^{129}Xe polarization vs. gas flow rate through the cell. The red line represents the modeled polarization for different gas flow rates (residency times), where a theoretical spin-exchange rate, $\gamma_{\mathrm{SE}}^{\mathrm{theory}}$, of 0.0033 Hz was used along with a theoretical equilibrium polarization (infinite residency time) of 86%. The blue line shows a fit (using Eq. (5)) to the experimental polarization data. From the fit, an empirical value for the spin-exchange rate, $\gamma_{\mathrm{SE}}^{\mathrm{emp}}$, was extrapolated to be 0.022 Hz, giving an empirical spin-exchange time of $\tau_{\mathrm{emp}} = 1/\gamma_{\mathrm{SE}}^{\mathrm{emp}} = 45$ s. Black dotted line indicates the flow rate of 650 sccm for which the residency time, t_{res}, of the gas in the cell is equal to the empirical spin-exchange time.

would be when performing *in vivo* MRI experiments with larger volumes of HP ^{129}Xe.

C. Modeling

A simple computational model was produced in order to compare established optical pumping efficiency theory with our experimental findings. The model uses MATLAB code (Mathworks, Natick, MA) to solve the numerical integral for the optical pumping rate, γ_{opt} (Eq. (2)), which is solved for discrete values along the z-axis (laser propagation direction).[14,15,39] The value of γ_{opt} is then used to calculate the alkali polarization (Eq. (1)) and hence the ^{129}Xe polarization (Eq. (5)). The Rb D_1 linewidth was estimated from Romalis *et al.*,[20] where a value of ~26 GHz (0.05 nm) was calculated based on an 18 GHz/amg broadening for a gas mixture of density 1.44 amg. The spin-destruction and spin-exchange cross sections used are as given in Eqs. (3), (4), and (6). The alkali density [Rb], was determined from the Killian formula[32] assuming oven temperature as measured with a thermocouple at the cell wall. The laser wavelength was set to the peak of the D_1 absorption (794.77 nm) and a laser FWHM of 0.09 nm was assumed based on measurement. Detailed experimental determination of [Rb] was not possible, and in a realistic case should be affected by laser heating,[40] as should the gas temperature in the cell. Nevertheless, the assumption of optical pumping with a cell at nominal temperature equilibrated with that of the oven provides a starting point for the modeling. See appendix for full details of modeling.

D. Polarization vs. flow rate

3% Xe was polarized in continuous-flow mode at different gas flow rates through the cell. At each gas flow rate, the gas was collected directly from the cell and a signal was acquired from a HP ^{129}Xe sample on the 1.5 T MRI system, as described above. Following each change in flow rate, the gas mixture was flowed through the cell for 5 min to allow for any laser heating effects to stabilize and to achieve a steady flow-rate-specific polarization level within the cell[40–42] prior to gas collection.

E. Accumulation of frozen Xe

The T_1 of frozen Xe in the freeze-out glassware was next investigated. At a fixed flow rate of 300 sccm, the Xe mixture exiting the cell was collected in cryogenic glassware made from Pyrex glass with a spiral shape (Fig. 4(a)), whereupon the gas mixture would enter the glassware flowing around and down the rings, deposit frozen Xe, and exit up through the vertical return tube in the center of the spiral.

The permanent magnet produced a static field of 0.3 T across the glassware and the path of the Xe from the cell to the glassware was routed through 6.35 mm (outer diameter) Tygon tubing (Saint-Gobain, France). The path was checked for magnetic field inhomogeneity using a Hall probe (GM08 Gaussmeter, Hirst Magnetics, Falmouth, UK). The permanent magnet's field did not vary more than 0.01 T per cm^3 over the volume within which the cryogenic glassware is kept during freeze-out, so it can be assumed to be sufficiently homogeneous so as not to cause significant T_1 shortening.[43]

After 10 min of frozen Xe accumulation, gas flow through the cell was stopped and the Xe was kept frozen within the cryogenic glassware for a range of storage times, t_s. During this time, liquid nitrogen in the Dewar was maintained at a constant level. Each storage-time batch of frozen Xe was sublimated into a Tedlar bag by immersion of the glassware in warm water and transported to the 1.5 T system for signal acquisition. In the above procedure, it was assumed that any potential polarization losses due to the frozen Xe's solid-gas phase transition would be the same for each t_s-accumulation as the volume of Xe collected is the same. A T_1 for the frozen Xe was calculated by fitting the decrease in FID signal amplitude to an exponential decay over increasing storage times, t_s (Figure 4(b)).

F. Photon efficiency

A theoretical photon efficiency was calculated by adapting the spin transfer efficiency formula derived by Bhaskar *et al.*[44] so that it includes vdW cross sections for spin-exchange and spin-destruction

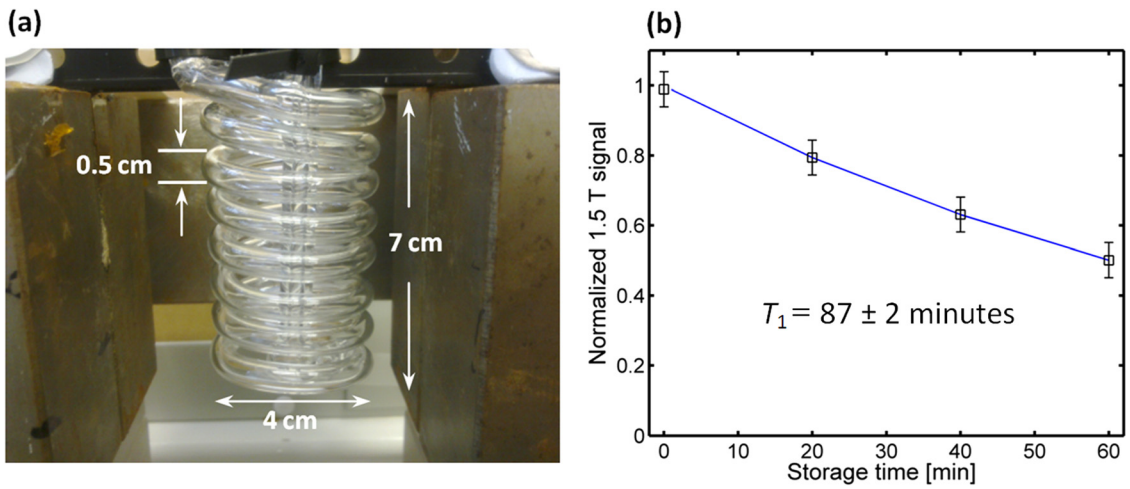

FIG. 4. (a) Freeze-out cryogenic glassware within holding magnetic field of ~0.3 T. (b) T_1 of frozen Xe held within the freeze-out glassware. A T_1 of 87 ± 2 min was estimated by performing an exponential fit (blue line) to the FID signal decrease as a function of storage time.

$$\eta_{\text{theory}} = \frac{\kappa_{\text{SE}}^{\text{BC,vdW}}}{\kappa_{\text{SD}}^{\text{BC,vdW}} + f\kappa_{\text{SE}}^{\text{BC,vdW}}} = \frac{\kappa_{\text{SE}}^{\text{BC}} + \kappa_{\text{SE}}^{\text{vdW}}}{(\kappa_{\text{SD}}^{\text{Rb-Xe}} + \kappa_{\text{SD}}^{\text{vdW}}) + f(\kappa_{\text{SE}}^{\text{BC}} + \kappa_{\text{SE}}^{\text{vdW}})}, \quad (8)$$

where f is the enrichment fraction (0.86) of ^{129}Xe. It is worth noting that Bhaskar *et al*. calculated the spin transfer efficiency by considering only binary Rb-Xe spin cross sections and concluded the efficiency to be independent of both laser power and temperature. An experimental photon efficiency, η_{exp}, defined as the ratio of ^{129}Xe polarization rate to the photon absorption rate in the cell volume, V, was determined under flow conditions (for a gas-residency time, t_{res}, equal to an empirically determined spin-exchange time, τ_{emp}—see Fig. 3) and was calculated using[45]

$$\eta_{\text{exp}} = \frac{[\text{Xe}]VP_{\text{Xe}}^{\tau_{\text{emp}}}/\tau_{\text{emp}}}{\Delta\phi}, \quad (9)$$

where $\Delta\phi$ is the number of photons being absorbed within the cell volume per second and $P_{\text{Xe}}^{\tau_{\text{emp}}}$ is the ^{129}Xe polarization measured at a flow rate of $\sim$650 sccm. The laser power transmitted through to the back of the cell was measured while the SEOP gas mixture was flowing through the cell at $\sim$650 sccm. Measurements were made while the cell was cold (293 K), P_{cold}, and hot (373 K), P_{hot}, and $\Delta\phi$ was calculated from $\Delta\phi(\lambda, T) = (P_{\text{cold}} - P_{\text{hot}})/E_P$, where E_P is the energy of a single photon carried within the laser beam with an emission centre wavelength of 794.77 nm.

G. Polarization vs. accumulation time

During freeze-out, a given volume of Xe is collected for a length of time defined as the accumulation time, t_{a}. It would be expected during a freeze-out procedure that, for a given t_{a}, a ^{129}Xe spin-ensemble contained within a layer of the Xe sample that was frozen at an earlier time would have undergone a greater amount of spin-lattice relaxation compared to spins in a layer of ^{129}Xe frozen at a later time, resulting in lower and higher polarization values in the respective layers. After time t_{a}, the frozen sample is sublimated into the gas phase and collected in a Tedlar plastic bag, resulting in mixing and an averaged polarization of the ^{129}Xe spin-ensemble within the bulk Xe gas mixture given by[16]

$$P_{\text{Xe}}^{\text{acc}}(t_{\text{res}}, t_{\text{a}}) = P_{\text{Xe}}^{\text{cell}}(t_{\text{res}})\frac{T_1}{t_{\text{a}}}(1 - \text{e}^{-\frac{t_{\text{a}}}{T_1}}), \quad (10)$$

where $P_{\text{Xe}}^{\text{cell}}$ is the ^{129}Xe polarization exiting the cell after a given residency time, t_{res}, and entering the glassware at $t_{\text{a}} = 0$ (Eq. (5)). To experimentally obtain $P_{\text{Xe}}^{\text{acc}}$, Xe was collected in the glassware during a continuous-flow freeze-out for different accumulation times in the range 10–60 min. Upon reaching the end of each t_{a}, the frozen Xe was sublimated into a Tedlar bag and transported to the 1.5 T MR system for signal acquisition.

H. *In vivo* ^{129}Xe lung MRI

^{129}Xe lung ventilation images were acquired with varying polarizations and inhaled volumes of ^{129}Xe. The gaseous volumes of enriched Xe (86% ^{129}Xe) collected were 300, 400, 600, and 800 ml (see Fig. 6 for the respective production rates and freeze-out accumulation times for each of the sample volumes). The Tedlar bag containing the thawed-out Xe was topped up to 1 l with medical grade N_2. All of the ^{129}Xe was polarized for human inhalation under a site-specific UK regulatory manufacturing licence from the MHRA. Lung MRI imaging was performed using a 3 T Philips Achieva system (Philips, Best, Netherlands) with quadrature flex T-R coils (CMRS, Brookfield, WI) on a healthy female volunteer (26 years old) with written consent and approval from the National Research Ethics Committee. A 2D spoiled gradient echo sequence was used. Sequence details: 96×96 matrix size; field of view 384×384 mm; slice thickness 15 mm; receive bandwidth 15.6 kHz; echo time 4.1 ms; repetition time 18.2 ms; flip angle 9°. Centric phase encode ordering was used to maximize the obtainable signal-to-noise ratio (SNR).[46]

III. RESULTS AND DISCUSSION

The results of temperature optimization under gas flow show that the cell gave optimum polarization when it was held at a temperature of 373 K (Fig. 2(a)). This is slightly offset from the modeling, which gave a similar temperature dependence, but instead predicted an optimum temperature under gas flow of 385 K (Fig. 2(b)). This offset is most likely due to the temperature of gas in the cell not being the same as the experimentally measured oven temperature of 373 K due to laser heating effects, which are discussed below. With the temperature set at 373 K, the ^{129}Xe polarization was found to decrease non-linearly as the gas flow rate through the cell was increased, consistent with earlier findings.[15,33,47] An exponential fit to the build-up portion of Eq. (5), $(1 - e^{-(\gamma_{\text{SE}}+\Gamma)t_{\text{res}}})$, was used to estimate an empirical value for the spin-exchange rate, $\gamma_{\text{SE}}^{\text{emp}}$, of 0.022 Hz, which is an order of magnitude higher than the calculated theoretical value (Eq. (6) and Table I) of 0.0033 Hz. In order to estimate the expected polarization for a cell temperature of 373 K and pressure of 2 bars, a simple model that utilizes the spin-exchange and destructions rates (Eqs. (2)–(4) and (6)) was used along with a simple numerical integration of the optical absorption of the laser light along the cell.[48] $P_{\text{Xe}}^{\text{cell}}$ was modelled for different cell residency times (flow rates) by using the theoretical spin-exchange rate, $\gamma_{\text{SE}}^{\text{theory}}$ (Table I), a theoretical Rb polarization, $\langle P_{\text{Rb}} \rangle$, of 95% and a ^{129}Xe spin destruction rate, Γ, equal to $1/T_1^{\text{cell}} = 3.5 \times 10^{-4}$ Hz. For a typical operating flow rate of 300 sccm, the theoretical ^{129}Xe polarization was calculated to be 24%, which is approximately a factor of 2 larger than the experimentally measured polarization of 12 ± 1% (Fig. 3). Also, the theoretical and experimentally measured ^{129}Xe polarization curves (Fig. 3) diverge at low flow rates. At low flow rates, gas in the cell has a greater amount of time to undergo heat exchange and is therefore more prone to laser heating effects (Walter *et al*.[40] found in a cell without gas flow that the cell temperature increased by approximately 105 K when 15 W of laser light

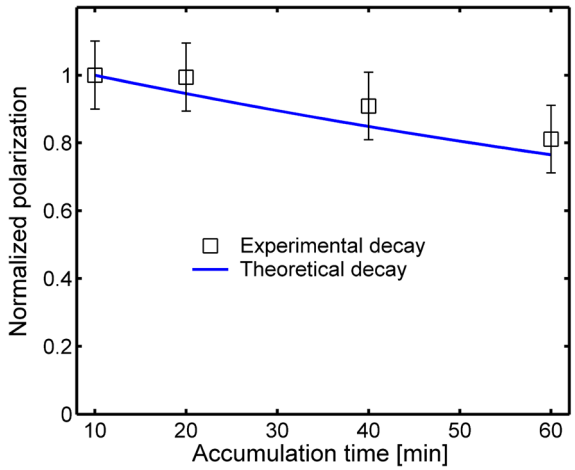

FIG. 5. Normalized 1.5 T signal vs. freeze-out accumulation time. The blue line represents the theoretical polarization decay with accumulation time (Eq. (10)).

was incident on the cell). The photon flux is most intense at the front of the cell and thus laser heating may cause an increase in [Rb] at the cell front. With a relatively long cell length of 25 cm, this could lead to a "hot-spot" of [Rb] resulting in fewer Rb exchange sites for ^{129}Xe nuclei traversing the cell length, as a result decreasing the average ^{129}Xe polarization. Indeed, EPR was recently used[15] to probe spatial inhomogeneity in the alkali polarization, which showed an area of depleted Rb polarization along the z-axis of a cylindrical cell.

The transmitted laser power was measured at 13.7 W and 7.8 W when the cell was cold (293 K) and hot (373 K), respectively, giving an absorbed laser power of 5.9 W (43%) and therefore a photon absorption rate, $\Delta\phi$, of 2.36×10^{19} photons per second (at 650 sccm). Given that the FWHM of the laser (~0.1 nm) is not much greater than pressure broadened Rb D_1 linewidth in the cell (0.05 nm), it can be assumed that the laser and cell are well matched for efficient optical pumping. Despite this, it is worth noting that the laser power incident upon the cell was measured to be ~25 W, whereas the laser power measured at the back of the cold cell was measured to be only 13.7 W. The loss in power here is assumed to be a result of scattering and reflection of the laser light from the cell walls and also from the glass windows of the oven. A theoretical photon efficiency, η_{theory}, was calculated (Eq. (8)) to be 0.039, lower than the previously reported theoretical efficiency of 0.043.[44] Whereas the spin transfer efficiency was previously considered to be temperature independent,[44] both the binary and vdW spin-destruction cross sections calculated in this study are dependent upon T, thus rendering a theoretical photon efficiency changes with temperature, which may explain the difference in the theoretical efficiency previously reported and the theoretical efficiency calculated here. Using Eq. (9), an experimentally determined photon efficiency was calculated for a gas mixture flowing through the cell ($T = 373$ K) at a rate of 650 sccm (the flow rate at which $t_{\text{res}} = 1/\gamma_{\text{SE}}^{\text{emp}} = \tau_{\text{emp}} = 45$ s). The polarization (Fig. 3) at this flow rate was measured as 8.6%, giving a $P_{\text{Xe}}^{\tau_{\text{emp}}}$ value in Eq. (9) of 0.086. Using the measured photon absorption rate, $\Delta\phi$, a ^{129}Xe fraction, f, of 0.86 and a cell volume of 491 cm^3 gives an experimental photon efficiency, $\eta_{\text{exp}} = 0.046$, which is in reasonable agreement with the theoretical value, $\eta_{\text{theory}} = 0.039$. Experimentally and theoretically, therefore, $1/\eta_{\text{exp}} = 22$ and $1/\eta_{\text{theory}} = 26$ photons are required per ^{129}Xe spin flip.

The T_1 of the frozen ^{129}Xe (see Fig. 4(b)) was calculated as 87 ± 2 min. This value is lower than what has previously been measured at a similar temperature and magnetic field in a recent solid-state ^{129}Xe NMR experiment,[49] where a value of ~2.5 h was reported. In an earlier study,[50] a T_1 for solid-state Xe was also reported to be ~2.5 h and it was concluded that below a temperature of 120 K, and above 55 K (Debye temperature for Xe, the temperature above which phonons are free to move), the interaction thought to be dominant for Xe relaxation in its frozen state is an inelastic spin-phonon scattering process resulting from a nuclear spin-rotation interaction. For those solid-state ^{129}Xe T_1 measurements,[49–51] Xe held within a glass cell was submerged as a bulk sample in liquid N_2, which is thought to result in the formation of a rigid-lattice face centred cubic polycrystalline solid. For Xe freezing under flow in spiral cryogenic glassware, such as in our system, the resulting Xe frost that is formed is less dense and may be prone to additional relaxation effects from the diffusion of gaseous oxygen into the frost.[52] Indeed oxygen may well be present in the circuit given the vacuum of ~4 mbar. Without *in situ* T_1 measurements of the frozen ^{129}Xe, these explanations for a lower than previously reported T_1 are somewhat speculative. Nevertheless, the value reported here is still encouragingly long, allowing for high SNR (~100) images from HP ^{129}Xe accumulated over a long accumulation time of 80 min (see Fig. 6(d)).

Fig. 5 shows a predicted model of the ^{129}Xe polarization, $P_{\text{Xe}}^{\text{acc}}$, (Eq. (10)) decay during accumulation. Using the

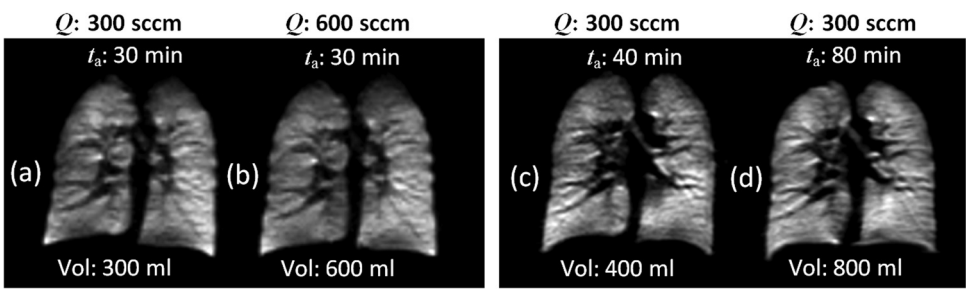

FIG. 6. *In vivo* gas-phase human lung images from a healthy volunteer at 3 T. (a) and (b) are 2D images of HP ^{129}Xe acquired from isotopically enriched gas mixtures (86% ^{129}Xe) flowed through the cell at volumetric flow rates (Q) of 300 and 600 sccm; (c) and (d) are 3D images of HP ^{129}Xe, both produced at a flow rate of 300 sccm for different accumulation times, t_a. Respective SNR values calculated for lungs in images (a), (b), (c), and (d) are 56, 52, 49, and 102.

measured T_1 value of 87 ± 2 min in the model shows good agreement with the experimental data. The percentage loss in the polarization is approximately 10% within an accumulation time of 40 min, which is typical of the time needed on this SEOP system to produce 400 ml Xe volumes for *in vivo* studies.

The ^{129}Xe gas ventilation images in Figs. 6(a) and 6(b) demonstrate that an image from a smaller volume of ^{129}Xe produced at a lower gas flow rate results in comparable SNR (~ 50) to an image acquired with double the gas volume at a higher flow rate. In addition, Figs. 6(c) and 6(d) show that for a given flow rate of 300 sccm, doubling the accumulation time, and therefore the volume of HP ^{129}Xe, results in an image with approximately double the SNR (increase from 50 to 100), confirming that T_1 losses during extended freeze-out periods are not a major concern.

IV. CONCLUSIONS

In this work, it has been shown a large volume cell (491 cm^3) operating at a mid-range pressure (2 bars with a 3% Xe mix) works well in combination with a spectrally narrowed laser in a SEOP system for production of HP ^{129}Xe (>10% ^{129}Xe polarizations) for *in vivo* lung MRI. The theoretical and experimental photon efficiencies, η_{theory} and η_{exp}, were calculated to be in good agreement with each other and indicate that $\sim$25 photons are required to induce each ^{129}Xe spin flip. The theoretical and experimental ^{129}Xe polarizations, however, are not in such good agreement and diverge at low flow rates, suggesting a break down in the theoretical model for long gas residency times which could be due to Rb runaway caused by laser heating.

Image SNR comparisons show that low volumes (<400 ml) of HP ^{129}Xe gas polarized can provide high quality ^{129}Xe lung MRI. The system has been running for $\sim$1 yr producing $\sim$400 ml gas samples for >100 *in vivo* ^{129}Xe lung imaging studies.

ACKNOWLEDGMENTS

We would like to thank Bastiaan Driehuys at Duke University for useful discussions on freeze-out and information on the 0.3 T storage magnet design and also for very helpful comments during the review process. We would also like to thank Helen Marshall for assistance in performing some of the *in vivo* imaging work in this paper. This work was funded by UK EPSRC Grant No. EP/D070252/1. Graham Norquay was funded on a Programme Grant No. C1276/A10345 from Cancer Research UK and EPSRC with additional funding from MRC and Department of Health (England) and we acknowledge the support of Professor Gill Tozer in this programme.

APPENDIX: OPTICAL PUMPING RATE MODEL

The optical pumping rate is dependent on the photon absorption cross section, σ_s, and on the photon flux from the laser, Φ, traversing the cell length z and defined by Eq. (2) as

$$\gamma_{\text{opt}}(z,\nu) = \int \Phi(z,\nu)\sigma_s(\nu)\mathrm{d}\nu.$$

The photon absorption cross section has a Lorentzian lineshape that varies with frequency, ν, according to[39]

$$\sigma_s(\nu) = \sigma_0 \frac{\Gamma_{\text{Rb}}^2}{4(\nu - \nu_{D_1})^2 + \Gamma_{\text{Rb}}^2}, \tag{A1}$$

where Γ_{Rb} is the FWHM of the pressure-broadened Rb electron D_1 Lorentzian line ($\sim$26 GHz for 1.44 amg gas density) with a peak amplitude $\sigma_0 = 2r_e cf/\Gamma_{\text{Rb}}$ and center frequency, ν_{D_1}. Here r_e is the classical electron radius, c is the speed of light and f is the oscillator strength of the D_1 transition, which has been found to be 0.337.[53] We have estimated the photon flux to vary with z and ν according to

$$\Phi(z,\nu) = I(\nu)e^{(-\lambda^{-1}(z,\nu)z)}, \tag{A2.1}$$

where $I(\nu)$ defines a Gaussian beam with an intensity that varies with frequency according to

$$I(\nu) = I_0 \mathrm{e}^{-\left(\frac{\nu-\nu_{\text{las}}}{\Gamma_{\text{las}}}\right)^2}. \tag{A2.2}$$

$I_0 = P/Ah\sqrt{\pi}\Gamma_{\text{las}}\nu_{\text{las}}$ gives the beam intensity on the cell front with P denoting the incident power on a flat cell face of cross sectional area, A. h is Planck's constant and Γ_{las} is the standard deviation of the Gaussian laser spectrum with centre frequency ν_{las}. λ^{-1} is the position-dependent absorption length, which for a circularly polarized beam with positive helicity, σ^+, illuminating the cell is given by[39]

$$\lambda^{-1}(z,\nu) = \sigma_s(\nu)[\text{Rb}](1 - P_{\text{Rb}}(z)). \tag{A2.3}$$

Equations (A1), (A2.1), and (A2.2) can be combined to give an expression for the optical pumping rate that can be solved numerically with a Simpson's integral over a frequency range $[\nu_{\text{min}}, \nu_{\text{max}}]$ for discrete z values

$$\gamma_{\text{opt}}(z,\nu) = \int_{\nu_{\text{min}}}^{\nu_{\text{max}}} I_0 \mathrm{e}^{-\left(\frac{\nu-\nu_{\text{las}}}{\Gamma_{\text{las}}}\right)^2} \mathrm{e}^{(-\lambda^{-1}z)} \sigma_0 \frac{\Gamma_{\text{Rb}}^2}{4(\nu - \nu_{D_1})^2 + \Gamma_{\text{Rb}}^2}\mathrm{d}\nu, \tag{A3}$$

where $\nu_{\text{min}} = \nu_{\text{las}} - 5\Gamma_{\text{las}}$ and $\nu_{\text{max}} = \nu_{\text{las}} + 5\Gamma_{\text{las}}$. This integration was performed for 25 values of z in increments of 1 cm for a 25 cm cell. The Rb polarization could then be calculated using Eq. (1) for each z value, whereupon an average Rb polarization was estimated by summing the calculated values and dividing by cell length. The average Rb polarization, $\langle P_{\text{Rb}} \rangle$, was then used to estimate the ^{129}Xe polarization for a range of cell temperatures and flow rates (e.g., see Figs. 2 and 3 for modeled ^{129}Xe polarizations).

NB: Chann *et al.* demonstrated skew-light effects on the light absorption efficiency at very small angles. With minimal skew-light observed with our ECDL, these effects have not been included in the modeling.

[1]T. G. Walker and W. Happer, Rev. Mod. Phys. **69**(2), 629–642 (1997).
[2]S. Patz, I. Muradyan, M. I. Hrovat, M. Dabaghyan, G. R. Washko, H. Hatabu, and J. P. Butler, New J. Phys. **13**, 015009 (2011).
[3]J. P. Mugler, T. A. Altes, I. C. Ruset, I. M. Dregely, J. F. Mata, G. W. Miller, S. Ketel, J. Ketel, F. W. Hersman, and K. Ruppert, Proc. Natl. Acad. Sci. U.S.A. **107**(50), 21707–21712 (2010).
[4]A. J. Swift, J. M. Wild, S. Fichele, N. Woodhouse, S. Fleming, J. Waterhouse, R. A. Lawson, M. N. Paley, and E. J. Van Beek, Eur. J. Radiol. **54**(3), 352–358 (2005).
[5]S. B. Fain, S. R. Panth, M. D. Evans, A. L. Wentland, J. H. Holmes, F. R. Korosec, M. J. O'Brien, H. Fountaine, and T. M. Grist, Radiology **239**(3), 875–883 (2006).
[6]E. J. van Beek, C. Hill, N. Woodhouse, S. Fichele, S. Fleming, B. Howe, S. Bott, J. M. Wild, and C. J. Taylor, Eur. Radiol. **17**(4), 1018–1024 (2007).
[7]A. Cho, Science **326**(5954), 778–779 (2009).
[8]M. S. Albert, G. D. Cates, B. Driehuys, W. Happer, B. Saam, C. S. Springer, Jr., and A. Wishnia, Nature **370**(6486), 199–201 (1994).
[9]B. Driehuys, G. P. Cofer, J. Pollaro, J. B. Mackel, L. W. Hedlund, and G. A. Johnson, Proc. Natl. Acad. Sci. U.S.A. **103**(48), 18278–18283 (2006).
[10]G. Duhamel, P. Choquet, E. Grillon, J. L. Leviel, M. Decorps, A. Ziegler, and A. Constantinesco, Acad. Radiol. **9**, S498–S500 (2002).
[11]B. Driehuys, H. E. Moller, Z. I. Cleveland, J. Pollaro, and L. W. Hedlund, Radiology **252**(2), 386–393 (2009).
[12]S. S. Kaushik, Z. I. Cleveland, G. P. Cofer, G. Metz, D. Beaver, J. Nouls, M. Kraft, W. Auffermann, J. Wolber, H. P. McAdams, and B. Driehuys, Magn. Reson. Med. **65**(4), 1154–1165 (2011).
[13]I. Dregely, J. P. Mugler III, I. C. Ruset, T. A. Altes, J. F. Mata, G. W. Miller, J. Ketel, S. Ketel, J. Distelbrink, F. W. Hersman, and K. Ruppert, J. Magn. Reson. Imaging **33**(5), 1052–1062 (2011).
[14]I. C. Ruset, S. Ketel, and F. W. Hersman, Phys. Rev. Lett. **96**(5), 053002 (2006).
[15]G. Schrank, Z. Ma, A. Schoeck, and B. Saam, Phys. Rev. A **80**(6), 063424 (2009).
[16]B. Driehuys, G. D. Cates, E. Miron, K. Sauer, D. K. Walter, and W. Happer, Appl. Phys. Lett. **69**(12), 1668–1670 (1996).
[17]A. L. Zook, B. B. Adhyaru, and C. R. Bowers, J. Magn. Reson. **159**(2), 175–182 (2002).
[18]W. Happer, E. Miron, S. Schaefer, D. Schreiber, W. A. Vanwijngaarden, and X. Zeng, Phys. Rev. A **29**(6), 3092–3110 (1984).
[19]W. Happer, Rev. Mod. Phys. **44**(2), 169 (1972).
[20]M. V. Romalis, E. Miron, and G. D. Cates, Phys. Rev. A **56**(6), 4569–4578 (1997).
[21]W. Happer and W. A. Vanwijngaarden, Hyperfine Interact. **38**(1-4), 435–470 (1987).
[22]A. B. A. Baranga, S. Appelt, M. V. Romalis, C. J. Erickson, A. R. Young, G. D. Cates, and W. Happer, Phys. Rev. Lett. **80**(13), 2801–2804 (1998).
[23]W. C. Chen, T. R. Gentile, T. G. Walker, and E. Babcock, Phys. Rev. A **75**(1), 013416 (2007).
[24]I. A. Nelson and T. G. Walker, Phys. Rev. A **65**(1), 012712 (2002).
[25]I. C. Ruset, Ph.D. dissertation, University of New Hampshire, 2005.
[26]B. Driehuys, G. D. Cates, and W. Happer, Phys. Rev. Lett. **74**(24), 4943–4946 (1995).
[27]Y. Y. Jau, N. N. Kuzma, and W. Happer, Phys. Rev. A **67**(2), 022720 (2003).
[28]Y. Y. Jau, N. N. Kuzma, and W. Happer, Phys. Rev. A **66**(5), 052710 (2002).
[29]G. D. Cates, R. J. Fitzgerald, A. S. Barton, P. Bogorad, M. Gatzke, N. R. Newbury, and B. Saam, Phys. Rev. A **45**(7), 4631–4639 (1992).
[30]C. V. Rice and D. Raftery, J. Chem. Phys. **117**(12), 5632–5641 (2002).
[31]X. Zeng, Z. Wu, T. Call, E. Miron, D. Schreiber, and W. Happer, Phys. Rev. A **31**(1), 260–278 (1985).
[32]T. J. Killian, Phys. Rev. **27**(5), 578–587 (1926).
[33]F. W. Hersman, I. C. Ruset, S. Ketel, I. Muradian, S. D. Covrig, J. Distelbrink, W. Porter, D. Watt, J. Ketel, J. Brackett, A. Hope, and S. Patz, Acad. Radiol. **15**(6), 683–692 (2008).
[34]S. R. Parnell, E. B. Woolley, S. Boag, and C. D. Frost, Meas. Sci. Technol. **19**(4), 045601 (2008).
[35]B. Chann, I. Nelson, and T. G. Walker, Opt. Lett. **25**(18), 1352–1354 (2000).
[36]S. R. Parnell, M. H. Deppe, J. Parra-Robles, and J. M. Wild, J. Appl. Phys. **108**(6), 064908 (2010).
[37]S. R. Parnell, S. Boag, T. J. McKetterick, and J. M. Wild, J. Phys.: Conf. Ser. **294**(1), 012010 (2011).
[38]K. Teh, N. de Zanche, and J. M. Wild, J. Magn. Reson. **185**(1), 164–172 (2007).
[39]M. E. Wagshul and T. E. Chupp, Phys. Rev. A **49**(5), 3854–3869 (1994).
[40]D. K. Walter, W. M. Griffith, and W. Happer, Phys. Rev. Lett. **86**(15), 3264–3267 (2001).
[41]A. Fink, D. Baumer, and E. Brunner, Phys. Rev. A **72**(5), 053411 (2005).
[42]S. R. Parnell, M. H. Deppe, S. Ajraoui, J. Parra-Robles, S. Boag, and J. M. Wild, J. Appl. Phys. **107**(9), 094904 (2010).
[43]W. Zheng, Z. I. Cleveland, H. E. Möller, and B. Driehuys, J. Magn. Reson. **208**(2), 284–290 (2011).
[44]N. D. Bhaskar, W. Happer, and T. McClelland, Phys. Rev. Lett. **49**(1), 25–28 (1982).
[45]E. Babcock, I. Nelson, S. Kadlecek, B. Driehuys, L. W. Anderson, F. W. Hersman, and T. G. Walker, Phys. Rev. Lett. **91**(12), 123003 (2003).
[46]J. M. Wild, M. N. Paley, M. Viallon, W. G. Schreiber, E. J. van Beek, and P. D. Griffiths, Magn. Reson. Med. **47**(4), 687–695 (2002).
[47]A. Fink and E. Brunner, Appl. Phys. B: Lasers Opt. **89**(1), 65–71 (2007).
[48]M. E. Wagshul and T. E. Chupp, Phys. Rev. A **40**(8), 4447–4454 (1989).
[49]N. N. Kuzma, B. Patton, K. Raman, and W. Happer, Phys. Rev. Lett. **88**(14), 147602 (2002).
[50]G. D. Cates, D. R. Benton, M. Gatzke, W. Happer, K. C. Hasson, and N. R. Newbury, Phys. Rev. Lett. **65**(20), 2591–2594 (1990).
[51]M. Gatzke, G. D. Cates, B. Driehuys, D. Fox, W. Happer, and B. Saam, Phys. Rev. Lett. **70**(5), 690–693 (1993).
[52]M. Limes, Z. Ma, E. Sorte and B. Saam, paper presented at the Xemat, Dublin, 2012.
[53]B. Larson, O. Hausser, P. P. J. Delheij, D. M. Whittal, and D. Thiessen, Phys. Rev. A **44**(5), 3108–3118 (1991).